Bollettino di Geofisica Teorica ed Applicata Vol. 55, n. 1, pp. 69-83; March 2014
DOI 10.4430/bgta0112

Earthquake rates inferred from active faults and geodynamics: the case of the External Dinarides

M.M.C. Carafa and V. Kastelic

Istituto Nazionale di Geofisica e Vulcanologia, L'Aquila, Italy

(Received: June 22, 2012; accepted: May 3, 2013)

ABSTRACT The goal of earthquake rate models is to define the number of earthquakes in a given time period above an established magnitude threshold. No earthquake rate models exist for the External Dinarides, although this area is prone to frequent earthquakes that have significant impacts on natural and human environments. In this study, we apply a tectonic/geodynamic approach to build a fault-based and a deformation-based earthquake rate model for the External Dinarides. The main difference between the two models is the inclusion of off-fault seismicity in the deformation-based earthquake rate model. We explore the impact of the moment-balancing uncertainties on the expected number of earthquakes. The results show comparable earthquake rates for both input models. The slip rate, the elastic modulus and the coupled thickness of the seismogenic lithosphere play important role in the variability of earthquake rates, whereas the effects of the corner magnitude and the Gutenberg - Richter β parameter are insignificant. A comparison with the available historical seismic catalogue shows good agreement for $M_W > 5.8$ earthquakes.

Key words: active fault, geodynamics, moment rate, earthquake rate, seismic hazard, External Dinarides.

1. Introduction

Earthquake rate models are a fundamental element in seismic hazard studies. Earthquake rates can be calculated using various methods, from empiro-statistical to fault-based models (Jackson and Kagan, 1999; Kagan and Jackson, 2000; Bird *et al*., 2002; Bird and Liu, 2007). The empiro-statistical methods project the historical seismicity into the future and calculate the seismic hazard regardless of the Earth's physical properties and processes. Whereas earthquake rates calculated from deformation models are constructed by considering characteristics of the seismic part of lithosphere. Both operations are affected by uncertainties (e.g., slip rate on faults or shear elastic modulus), which need to be considered to explore the earthquake rate variability.

To determine the parameters and related uncertainties of magnitude-frequency distributions, Bird and Kagan (2004) used the ergodic assumption: for globally uncorrelated seismicity, data collected over a broad area and over long time periods allow parameters to be determined at a local scale. Bird and Kagan (2004) determined the average magnitude-frequency distribution for each plate boundary type using the plate model of Bird (2003) and three different seismic catalogues [Harvard CMT catalogue: Pacheco and Sykes (1992), Ekström and Nettles (1997),

Ekström *et al*. (2012)]. Bird and Kagan (2004) have also shown that fundamental parameters in moment-rate balancing, such as coupled thickness (the product of the seismogenic lithosphere thickness and seismic coupling) and corner magnitude, are sensitive to fault kinematics. Furthermore, relationships between relative plate velocity and seismicity differ within the same plate-boundary class; for example, the earthquake rates and relative plate velocities at subduction zones have nonlinear relationships (Bird *et al*., 2009).

The Seismic Hazard Inferred From Tectonics (SHIFT) model (Bird and Liu, 2007; Howe and Bird, 2010) determines earthquake rates incorporating above described findings on plate tectonics and seismicity. SHIFT's main assumption is that the shallow seismicity along faults and zones of distributed anelastic strain can be predicted by treating them as a small sample of the corresponding plate boundary type (Bird and Kagan, 2004; Bird *et al*., 2009). In SHIFT the deforming-continua strain rates and fault slip rates are converted into moment rates, after which the seismicity properties of the corresponding plate boundary are used to calculate the earthquake rates. Similar studies using the SHIFT hypotheses for different regions have been carried out by Bird (2009), Rucker (2009) and Bird *et al*. (2010). The SHIFT earthquake rates are valuable, as they can be compared to the numbers of earthquakes reported in seismic catalogues.

In this work, we applied SHIFT to estimate the long-term average earthquake rate and related uncertainties for the seismically active thrust-and-fold belt of the External Dinarides (ED), which deforms at low rates (Grenerczy *et al*., 2005; Bennett *et al*., 2008; Kastelic and Carafa, 2012). We applied SHIFT to the deformation model of Kastelic and Carafa (2012) [Deformation (FEM) model] and to the ED part of the fault-based model of Basili *et al*. (2013) [Fault-based (GEO) model]. We determined the number of earthquakes and related uncertainties above the completeness threshold of the Harvard CMT catalogue (Ekström *et al*., 2012) for both models. The earthquake-rate maps show that the areas of greatest seismic deformation lie in the SE of the ED. From the earthquake rate calculations based on the FEM and GEO models, 3.6 and 3.1 $M_W > 5.66$ earthquakes in a century are expected to occur in the ED. The comparison with the earthquake catalogue shows that the number of registered earthquakes falls within the uncertainties of the FEM- and GEO-based earthquake rates.

2. Tectonic setting

The ED were formed by a progressive westward compression between the eastern Adria microplate and the Internal Dinarides (Tari, 2002). The oldest thrusting activity associated with the ED in western Slovenia was recorded by Early Eocene foredeep flysch deposits (Drobne and Pavlovec, 1991). The onset of thrusting and related foredeep flysch deposition becomes younger to the SE along the thrust belt and to the west toward the offshore region (Tari, 2002). Throughout the Oligocene-Miocene, the foredeep basins progressively occupied the Adriatic offshore area (Tari-Kovačić, 1998; Tari-Kovačić *et al*., 1998) and in the central Adriatic Sea, the outermost front of the NE-dipping ED lies adjacent to the SW-dipping northern Apennines outermost thrust front (Scrocca, 2006; Kastelic and Carafa, 2012; Kastelic *et al*., 2013). The active faults in the ED are mostly NW-SE and NE-dipping thrusts and are seismogenic throughout the belt (e.g., Shebalin *et al*., 1974; Herak *et al*., 1996; Grünthal and

Wahlström, 2012; Kastelic *et al.*, 2013; Stucchi *et al.*, 2013). Deformation rates are higher in the south-eastern portion of the ED, with slip and strain rates diminishing to the NW and lower deformation rates for areas offshore (Kastelic and Carafa, 2012). The low deformation rates for the central Adriatic may also be influenced by the stronger rheology of the Adriatic lithosphere with respect to its surrounding areas (Carafa and Barba, 2011).

3. Input data

3.1. Deformation (FEM) model

For the FEM model, we relied on the finite element geodynamic model developed for the ED (Kastelic and Carafa, 2012). This model takes into account the rheology, the velocity field and the fault friction of the ED. The 3D grid is defined in a dual-layered (crust and upper mantle) lithosphere containing 171 fault elements and 1591 spherical triangle elements. The geodynamic model (Kastelic and Carafa, 2012) was calibrated using several sets of geophysical and geodetic data and it is characterised by a mean error of 22.44° with respect to the horizontal stress orientation and a root mean square error of 1.4 mm/yr with respect to the available GPS measurements.

We incorporated the FEM model into this study using the position, geometry, slip rate and strain rate of both the fault and triangular continuum elements. We assumed the seismic deformation to be released either along the fault or within the continuum elements. The fault slip rates are a direct result of the numerical modelling technique (Kastelic and Carafa, 2012) and in this study we utilised the median, the 5^{th} and 95^{th} percentile values of slip rate to explore the sensitivity of earthquake rates with respect to fault slip rates. The median values of the fault elements are between 0.03 and 2.52 mm/yr, the 5^{th} percentile values are between 0.02 and 1.00 mm/yr and the 95^{th} percentile values are between 0.04 and 3.50 mm/yr.

3.2. Fault-based model (GEO)

The GEO model is based only on active fault data, whereas off-fault deformation is not considered. The active faults used in this model are a part of the European Database of the Seismogenic Faults (Basili and Kastelic, 2011; Basili *et al.*, 2013). This model of seismogenic sources represents the latest version of the DISS updated in the EP7 project "Seismic Hazard Harmonization in Europe - SHARE" and differs from the previous model in the larger number of the sources and, in certain cases, in the greater detail.

The GEO model contains 218 fault elements capable of hosting $M \geq 5.5$ earthquakes. For the seismic moment and earthquake rate calculations, we used the minimum, average and maximum slip rates. The variability of the minimum slip rates among all faults elements is 0.05 - 0.90 mm/yr, with average values of 0.10 - 1.45 mm/yr and maximum values of 0.15 - 2.00 mm/yr.

4. Earthquake rate calculations

The relationship between seismicity and the long-term (averaged over 10^5 years) fault behaviour is studied through the long-term average seismic moment rate. Following Bird and

Kagan (2004), we assumed that the relationship between plate tectonics and seismicity can be expressed as:

$$\frac{1}{R}\lim_{\Delta t\to\infty}\frac{\sum M}{\Delta t}=\int\int c\mu\dot{s}dA\,; \tag{1}$$

where R is the moment-recording factor of the seismic network ($0 < R \leq 1$), M is the seismic moment, t is the length of observation, c is the seismic coupling, defined as the fraction of frictional sliding that occurs in earthquakes, μ is the elastic shear modulus, $\dot{s}$ is the long-term slip rate of the fault and A is the area of the fault with a frictional-dominated rheology.

We calculated the seismic moment rates and earthquake rates separately for the FEM and the GEO models. Consistent with the SHIFT assumptions, the seismic deformation in the FEM model is released along the fault elements and within the spherical triangle continuum elements and thus the earthquake rates are calculated separately for each fault (as described in Section 4.1.) and for each continuum element (as described in Section 4.2.). In the fault-based GEO model, the seismic deformation is released only along the faults with earthquake rates calculated as described in Section 4.1.

4.1. Seismicity of faults

The seismic moment rate $\dot{M}_0^f\left(f,(\dot{s}_f)\right)$ of any fault f in the FEM or GEO model is defined as:

$$\dot{M}_0^f\left(f,\left(\dot{s}_f\right)\right)=\int\int c\mu\left(\dot{s}_f\right)dA\,, \tag{2}$$

where c is the seismic coupling factor, μ is the elastic shear modulus, $(\dot{s}_f)$ is the slip rate of fault f and A is the frictional portion of the fault area from the surface to the depth of the brittle-ductile transition. The slip rates for the FEM model $(\dot{s}_f)=(\dot{s}_{f_{FEM}})$ were taken from the results of the geodynamic model of Kastelic and Carafa (2012) and the slip rates for the GEO model $(\dot{s}_f)=(\dot{s}_{f_{GEO}})$ were taken from Basili *et al.* (2013). Both the FEM and GEO fault slip rates include their associated uncertainties. In the FEM model, the slip rate of each fault is the median $(\dot{s}_f)=(\dot{s}_{f_{FEM}})_{50th}$ of the models that minimise the SHmax orientations; the 5th $(\dot{s}_f)=(\dot{s}_{f_{FEM}})_{5th}$ and 95th $(\dot{s}_f)=(\dot{s}_{f_{FEM}})_{95th}$ percentile values define the uncertainty bounds. In the GEO model, the slip-rates uncertainty bounds are reported for each active fault in the minimum $(\dot{s}_f)=(\dot{s}_{f_{GEO}})_{\min}$ and maximum $(\dot{s}_f)=(\dot{s}_{f_{GEO}})_{\max}$ interval while we calculated the average value at the middle of this interval.

We underline that the FEM and GEO slip rate uncertainties are non-equivalent due to their different acquisition methods; for the FEM slip rate, the uncertainty bounds are defined by the 5th - 95th percentiles of dynamic models best-fitting SHmax orientations and GPS measurements, whereas in the GEO model, they represent the absolute minimum and maximum slip rates of the available data for each fault. These two quantities are formally different, but in both cases determined by considering similar kinematic indicators. For the sake of simplicity, we conceptually considered $(\dot{s}_{f_{GEO}})_{\min}$ as equivalent to $(\dot{s}_{f_{GEO}})_{5th}$ and $(\dot{s}_{f_{GEO}})_{\min}$ as equivalent to $(\dot{s}_{f_{GEO}})_{95th}$.

Assuming that the slip does not vary in the down-dip direction of the fault plane, we can rewrite Eq. (2) following the method of Bird and Kagan (2004):

$$\dot{M}_0^f\left(f,\dot{s}_f,\mu,\langle cz\rangle\right)\cong\langle cz\rangle\int_L\mu\sqrt{\left(v_P\left(f,\dot{s}_f\right)\right)^2+\left(v_O\left(f,\dot{s}_f\right)\sec\left(\theta_f\right)\right)^2}\csc\left(\theta_f\right)dl\,; \tag{3}$$

where $\langle cz\rangle$ is the coupled thickness of the seismogenic lithosphere, $v_P\left(f,(\dot{s}_f)\right)$ and $v_O\left(f,(\dot{s}_f)\right)$ sec (θ_f) are the slip rate components parallel and orthogonal to the strike of the fault, respectively, θ_f is the fault dip, dl is a small step along the length L of the fault and μ is the elastic shear modulus.

The effective variability in the moment rate for each FEM and GEO fault cannot be addressed without investigating the role of μ, $\langle cz\rangle$ and $(\dot{s}_f)$ uncertainties. For the ED faults, the unknown values in Eq. (3) are μ and $\langle cz\rangle$, thus we applied values and related uncertainties as given by Bird and Kagan (2004). As $\langle cz\rangle$ is highly variable for different types of plate boundaries, the assignment of each fault to a plate boundary type becomes fundamental. Based on the kinematics of FEM and GEO fault elements, the strike-slip faults were assigned to the Continental Transform Fault (CTF) type of plate boundary and thusts were assigned to the slow Continental Convergent Boundary (CCB slow) type.

The fully-explored variability in fault moment rate is given by $\dot{M}_0^f\left(f_{FEM},(\dot{s}_{f_{FEM}})_{5th},\mu_{\min},\langle cz\rangle_{\min}\right)$ - $\dot{M}_0^f\left(f_{FEM},(\dot{s}_{f_{FEM}})_{95th},\mu_{\min},\langle cz\rangle_{\min}\right)$ for the FEM model and by $\dot{M}_0^f\left(f_{GEO},(\dot{s}_{f_{GEO}})_{\min},\mu_{\min},\langle cz\rangle_{\min}\right)$ - $\dot{M}_0^f\left(f_{GEO},(\dot{s}_{f_{GEO}})_{\max},\mu_{\min},\langle cz\rangle_{\min}\right)$ for the GEO model.

After we obtained the long-term seismic moment rate $\dot{M}_0^f\left(f,(\dot{s}_f),\mu,\langle cz\rangle\right)$ and the related uncertainty, we calculated the number of earthquakes $\dot{N}^f(M_W>M_W^T,\mathrm{f},(\dot{s}_f),\mu,\langle cz\rangle,\beta,M_W^c)$ of M_W that exceed a threshold magnitude M_W^T, dividing the long-term seismic moment rate of each fault by the moment rate of the appropriate worldwide plate-type boundary sub-catalogue (Bird and Kagan, 2004). In the successive step, we multiplied the obtained value by the number of events $\dot{N}^f\left(M_W>(M_W^T)^{CMT}\right)$ exceeding the threshold magnitude M_W^T of the appropriate earthquake sub-catalogue. In the final step, the earthquake rates were adjusted to any chosen threshold magnitude M_W^T by applying the tapered Gutenberg-Richter distribution [Eq. (9): Bird and Kagan (2004)] as:

$$\dot{N}^f\left(M_W>M_W^T,f,\left(\dot{s}_f\right),\mu,\langle cz\rangle,\beta,M_W^c\right)=\left(\dot{M}_0^f\left(f,\left(\dot{s}_f\right),\mu,\langle cz\rangle\right)\Big/\dot{M}_0\left(\left(M_W^T\right)^{CMT}\right)\right)\cdot\dot{N}^{CMT}\cdot$$

$$\left(\frac{M_0\left(M_W^T\right)}{M_0\left(\left(M_W^T\right)^{CMT}\right)}\right)^{-\beta}\times\exp\left(\frac{M_0\left(\left(M_W^T\right)^{CMT}\right)-M_0\left(M_W^T\right)}{M_0\left(M_W^c\right)}\right), \tag{4}$$

where M_W^c is the corner magnitude and β is the asymptotic spectral slope for small moments. For each fault, both values were taken from the analogue plate boundary type (Bird and Kagan, 2004).

To determine the variability in earthquake rate for each fault, we also considered the uncertainties in β and M_W^c reported by Bird and Kagan (2004) for the CTF and CCB plate boundary types. All values used in the calculations are listed in Table 1.

As a final step in the earthquake rate calculations, we allowed the earthquake rate $\dot{N}^f(M_W>M_W^T,f,(\dot{s}_f),\mu,\langle cz\rangle,\beta,M_W^c)$ to be evenly distributed along the seismogenic portion of each fault plane, with the hypocentres projected to the surface. With the known length L, dip θ_f and seismogenic depth z of each fault corresponding to the appropriate plate boundary type (Bird

Table 1 - Seismicity parameters applied to fault elements (after Bird and Kagan, 2004; Bird *et al*., 2009).

		CTF			CCB		
Symbol	Represents	Minimum Value (X_{min})	Average Value (X_{avg})	Maximum Value (X_{max})	Minimum Value (X_{min})	Average Value (X_{avg})	Maximum Value (X_{max})
μ (GPa)	Shear elastic modulus	22.1	27.7	34	22.1	27.7	34
⟨*cx*⟩ (km)	Coupled thickness	0.38	0.72	1	0.51	0.84	1
β	Slope GR	0.53	0.65	0.77	0.52	0.62	0.72
m_c^*	Corner magnitude	7.54	8.01	8.22	8.07	8.46	8.67

and Kagan, 2004) (reported in Table 1), we can determine the productivity $EQ^f(M_W > M_W^T, f, \dot{s}_f, \mu, \langle cz \rangle, \beta, M_W^c)$ of a fault *f*:

$$EQ^f\left(M_W > M_W^T, f, \dot{s}_f, \mu, \langle cz \rangle, \beta, M_W^c\right) = \dot{N}^f\left(M_W > M_W^T, f, \left(\dot{s}_f\right), \mu, \langle cz \rangle, \beta, M_W^c\right) / L \cdot z / \tan(\theta)) \cdot \quad (5)$$

The number of events $\dot{N}^f(M_W > M_W^T, f, (\dot{s}_f), \mu, \langle cz \rangle, \beta, M_W^c)$ exceeding a certain threshold magnitude becomes uniformly distributed as a constant earthquake rate $EQ^f(M_W > M_W^T, f, \dot{s}_f, \mu, \langle cz \rangle, \beta, M_W^c)$ in a band that is $\Delta x\,(f) = z / \tan(\theta)$ wide around the fault trace with a length *L*.

4.2. Seismicity of deforming continua

The FEM deformation model, besides the slip rates for given faults, reports also deformation rates away from the explicitly modelled faults, which may indicate deformation on unknown faults. Kastelic and Carafa (2012) proposed that for the ED, the FEM-modelled continuum strain rate could contain deformation related to unidentified active faults. And thus, for the earthquake rate calculation, we included also the off-fault deformation of the FEM model.

The three orthogonal principle axes ($\dot{\varepsilon}_1 \le \dot{\varepsilon}_2 \le \dot{\varepsilon}_3$) and their principal values were used to determine the seismic moment rates due to the continuum elements. If we neglect phase and porosity changes, we can assume the lithosphere to be incompressible $\dot{\varepsilon}_1 + \dot{\varepsilon}_2 + \dot{\varepsilon}_3 = 0$, with one of the principal strain rates defined as vertical and calculated from the two horizontal principle strain rates $\dot{\varepsilon}_{vert} = -(\dot{\varepsilon}_{1h} + \dot{\varepsilon}_{2h})$. The incompressibility assumption infers that $\dot{\varepsilon}_1 < 0 < \dot{\varepsilon}_3$, with only the sign of $\dot{\varepsilon}_2$ varying. The magnitude of the vertical principal strain rate $\dot{\varepsilon}_{vert}$ relative to the two horizontal principal strain rates is used to determine the kinematics of the deforming continuum elements (thrusting, strike-slip, or normal faulting) and to assign each element to the most similar plate boundary type (see Table 2). The seismic moment rate for the seismogenic portion of any continuum element e_{FEM} was calculated following the method of Bird and Liu (2007):

$$\dot{M}_0^e\left(e_{FEM}, \mu, \langle cz \rangle\right) \cong = A\langle cz \rangle \mu \begin{Bmatrix} 2\dot{\varepsilon}_3; \text{if } \dot{\varepsilon}_2 < 0, \text{OR} \\ -2\dot{\varepsilon}_1; \text{if } \dot{\varepsilon}_2 \ge 0 \end{Bmatrix}, \quad (6)$$

where *A* represents the surface area of the continuum element e_{FEM}, $\langle cz \rangle = \langle cz \rangle_{agv}$ is the coupled thickness of the continuum element (with confidence interval $\langle cz \rangle_{\min} - \langle cz \rangle_{\max}$), μ_{avg} is the average elastic shear modulus (with confidence interval $\mu_{\min}$ - $\mu_{\max}$) and $\dot{\varepsilon}_1$, $\dot{\varepsilon}_2$ and $\dot{\varepsilon}_3$ are the principal axes

Table 2 - Seismicity parameters applied to the deforming continua (after Bird and Kagan, 2004).

Vertical strain rate	Plate boundary	Shear elastic modulus μ (GPa)			Coupled thickness $\langle cz \rangle$ (km)			Slope GR β			Corner magnitude $(M_W)_c$		
		μ_{min}	μ_{avg}	μ_{max}	$\langle cz \rangle_{min}$	$\langle cz \rangle_{avg}$	$\langle cz \rangle_{max}$	β_{min}	β_{avg}	β_{max}	$(M_W^c)_{min}$	$(M_W^c)_{avg}$	$(M_W^c)_{max}$
$\dot{\varepsilon}_{vert} > 0$ and $\dot{\varepsilon}_{vert} > 0.364 \cdot \dot{\varepsilon}_{2h}$	CCB	22.1	27.7	34	0.51	0.84	1.00	0.52	0.62	0.72	8.07	8.46	8.67
$\dot{\varepsilon}_{vert} > 0$ and $\dot{\varepsilon}_{vert} \leq 0.364 \cdot \dot{\varepsilon}_{2h}$ OR $\dot{\varepsilon}_{vert} > 0$ and $\dot{\varepsilon}_{vert} \geq 0.364 \cdot \dot{\varepsilon}_{1h}$	CTF	22.1	27.7	34	0.38	0.72	1.00	0.53	0.65	0.77	7.54	8.01	8.22

of the strain rate tensor. The values of A and the average values of $\dot{\varepsilon}_1$, $\dot{\varepsilon}_2$ and $\dot{\varepsilon}_3$ for each element were taken from the FEM model of Kastelic and Carafa (2012), although we did not explore the corresponding uncertainties because the strain rate release represents only 10% of the total deformation in the ED and is not considered a significant source of error. The remaining values (coupled thickness $\langle cz \rangle$, elastic shear modulus μ and asymptotic spectral slope β) were taken from the corresponding value of the plate boundary type, as previously determined for each element (Table 2).

The earthquake rate is calculated using:

$$\dot{N}^e\left(M_W > M_W^T, f, \left(\dot{s}_f\right), \mu, \langle cz \rangle, \beta, M_W^c\right) = \left(\dot{M}_0^e\left(e_{FEM}, \mu, \langle cz \rangle\right) \Big/ M_0\left(\left(M_W^T\right)^{CMT}\right)\right) \cdot \dot{N}^{CMT} \cdot$$

$$\cdot \left(\frac{M_0\left(M_W^T\right)}{M_0\left(\left(M_W^T\right)^{CMT}\right)}\right)^{-\beta} \times \exp\left(\frac{M_0\left(\left(M_W^T\right)^{CMT}\right) - M_0\left(M_W^T\right)}{M_0\left(M_W^c\right)}\right). \quad (7)$$

For each element, the bounds of the earthquake rate variability due to the uncertainties in μ and $\langle cz \rangle$ are $\dot{N}^e(M_W > M_W^T, e_{FEM}, \mu_{min}, \langle cz \rangle_{min}, (M_W^c)_{min})$ and $\dot{N}^e(M_W > M_W^T, e_{FEM}, \mu_{max}, \langle cz \rangle_{max}, (M_W^c)_{max})$. In the case of the deforming continuum element, the earthquake epicentres were uniformly distributed on the spherical-triangle finite element surface A (e_{FEM}) following:

$$EQ^e(M_W > M_W^T, e_{FEM}, \mu, \langle cz \rangle, \beta, M_W^c) = \dot{N}^e\left(M_W > M_W^T, e_{FEM}, \mu, \langle cz \rangle, \beta, M_W^c\right) / A(e_{FEM}). \quad (8)$$

To present our results as earthquake rates in map view (Figs. 2 and 3), we built a grid with 0.2° steps in latitude and longitude. For the GEO model, the earthquake rate EQ_p for each grid point p is given by the sum of all $EQ^f(M_W > M_W^T, f_{GEO}, \dot{s}_{f_{GEO}}, \mu, \langle cz \rangle, \beta, M_W^c)$ for faults in the area, with $L \cdot \Delta x$ (f_{GEO}), which contains the grid point p. For the FEM model, EQ_p is obtained by summing $EQ^f(M_W > M_W^T, f_{FEM}, \dot{s}_{f_{FEM}}, \mu, \langle cz \rangle, \beta, M_W^c)$ for the fault and $EQ^e(M_W > M_W^T, e_{FEM}, \mu, \langle cz \rangle, \beta, M_W^c)$ for the continuum elements, with an area of $L \cdot \Delta x$ (f_{FEM}) and a triangular area A (e_{FEM}) that contains the grid point p.

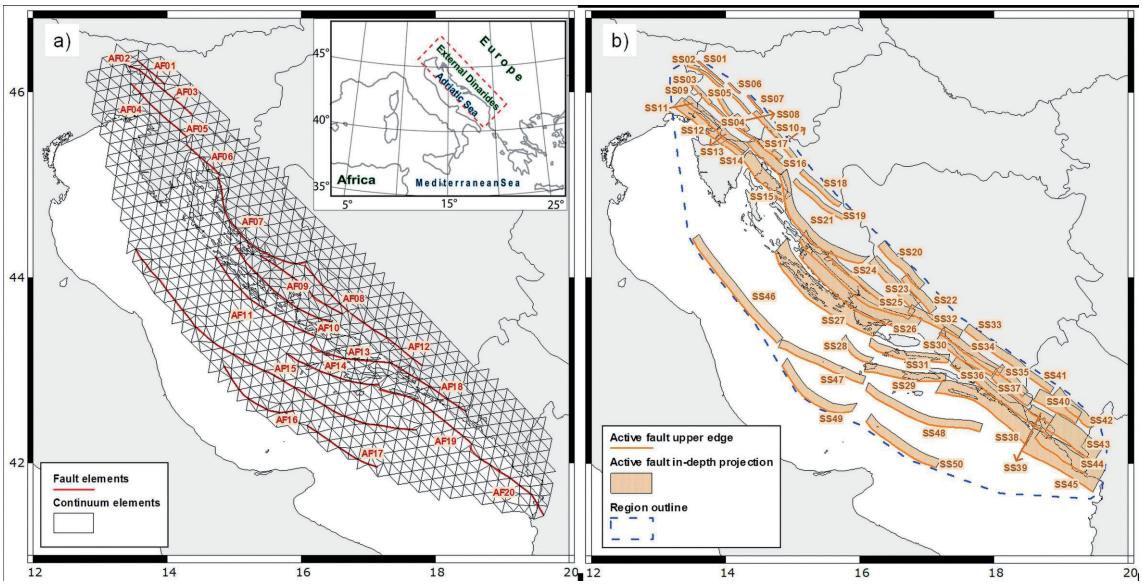

Fig. 1 - Input models used to calculate the long-term average moment and earthquake rates: a) Finite Element Model (FEM) (Kastelic and Carafa, 2012) composed of Fault Elements (AF) labelled with their code names (red lines) and continuum elements (black triangles). The inset highlights the study area (red dashed rectangle) and the principle structural units; b) fault-based model (GEO) (Basili *et al.*, 2013) in the investigated region (dashed blue polygon). The upper edges (orange lines) and down-dip planes (orange polygons) of labelled seismogenic sources are shown.

The sum of EQ_p integrated over the entire ED results in the total number of earthquakes in the form of $\dot{N}(M_W > M_W^T, FEM\ /\ GEO,\ \dot{s}_f, \mu, \langle cz \rangle, \beta, M_W^c)$, where *FEM* or *GEO* denotes the model used. We explored the effect of the parameter uncertainties in terms of the number of earthquakes of magnitude $M_W > M_W^T$ in a century (EQ/100 yr^{-1}) because we consider this approach to be the most direct and intuitive. As several of the input parameters and their related uncertainties were deduced from Bird and Kagan (2004), we chose $M_W^T = 5.66$ as the threshold magnitude in order to respect the seismic moment completeness threshold of $M_0 = 3.5 \times 10^{17}$ Nm for the CMT catalogue (Bird and Kagan, 2004).

We performed sensitivity analyses to study how the variability in the earthquake rates can be apportioned to different input uncertainties. For each input parameter ($\dot{s}_f$, μ, $\langle cz \rangle$, β, M_W^c), we used its minimum and maximum value to determine its influence on earthquake rate variability, as we kept the remaining parameters set to their average values (see Table 1). To avoid complex mathematical notations, we refer to the calculated earthquake rates using the minimum, average and maximum values of all input parameters as $\dot{N}^{\min}_{FEM/GEO}$, $\dot{N}^{agv}_{FEM/GEO}$ and $\dot{N}^{\max}_{FEM/GEO}$, respectively.

5. Results

Consistent with the SHIFT method, the assignment of the appropriate plate boundary type to the 171 fault elements resulted in 23 fault elements assigned to the CTF type and the remaining 148 assigned to the CCB slow-deforming plate boundary type. The majority (1511) of the continuum elements were assigned to the CCB slow-deforming plate boundary type and 80

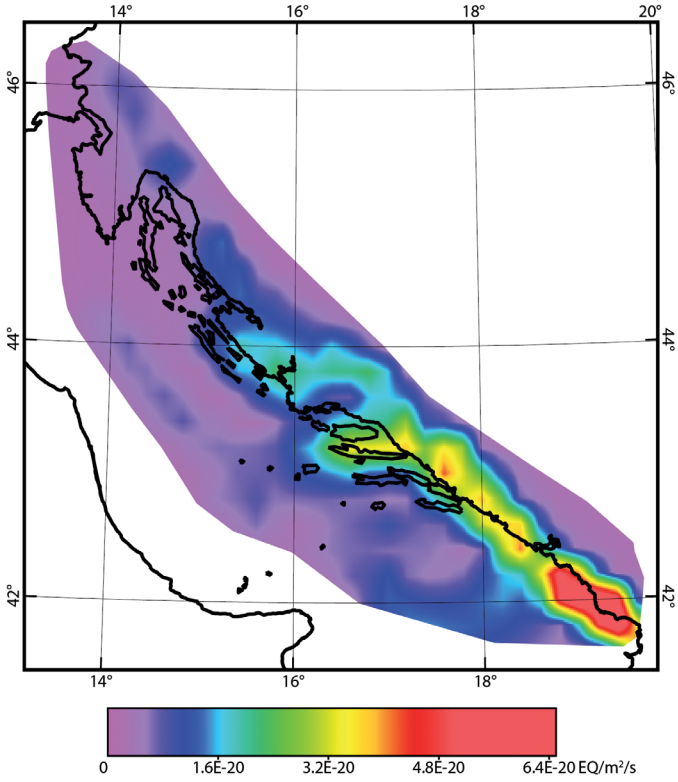

Fig. 2 - Earthquake rates of $M_W > 5.66$ (in EQ/m^2/s) in the ED calculated from the FEM model. Additional details can be found in the text.

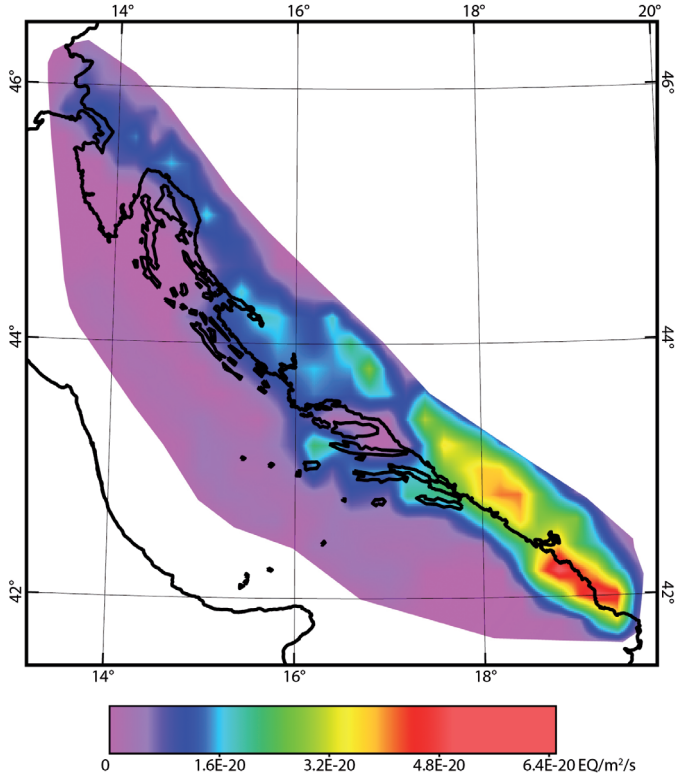

Fig. 3 - Earthquake rates of $M_W > 5.66$ (in EQ/m^2/s) in the ED calculated from the GEO model. Additional details can be found in the text.

were assigned the CTF plate boundary type. The earthquake rates calculated from the FEM and GEO models (Figs. 2 and 3) for M_W>5.66 are the highest in the south-eastern portion of the ED and generally diminish toward the NW, reaching a minimum in the north-westernmost portion of the ED.

The FEM model predicts average, minimum and maximum numbers of M_W>5.66 earthquakes of $\dot{N}^{agv}_{FEM}$ = 3.6 EQ/100 yr^{-1}, $\dot{N}^{\min}_{FEM}$ = 1.2 EQ/100 yr^{-1} and $\dot{N}^{\max}_{FEM}$ = 10.8 EQ/100 yr^{-1}, respectively (Fig. 4).

The earthquake-rates sensitivity analysis shows that M^c_W and β have a marginal impact on the predicted number of earthquakes. In contrast, uncertainties in μ have a greater impact on the number of earthquakes, causing rates to vary from 2.9 EQ/100 yr^{-1} to 4.5 EQ/100 yr^{-1}. Similarly, uncertainties in $\dot{s}_{f_{FEM}}$ cause rates to vary from 2.3 EQ/100 yr^{-1} to 5.3 EQ/100 yr^{-1}. Among the analysed parameters, $\langle cz \rangle$ has the largest effect on the earthquake rate, causing it to vary from 2.3 EQ/100 yr^{-1} to 6.0 EQ/100 yr^{-1} (Fig. 4).

The earthquake rates for the GEO model show a similar geographic trend to the FEM model (Fig. 3). Among the 50 seismogenic sources, 19 were assigned to the CTF and 31 to the CCB slow-deforming plate type boundary. The average number of M_W>5.66 earthquakes in a century resulted in $\dot{N}^{agv}_{GEO}$ = 3.1 EQ/100 yr^{-1}. The lower and upper bounds, respectively, are given by $\dot{N}^{\min}_{GEO}$ = 0.7 EQ/100 yr^{-1} and $\dot{N}^{\min}_{GEO}$ = 10.7 EQ/100 yr^{-1}. Similar to the FEM model, the uncertainties in M^c_W and β have little influence on the final earthquake rates. Uncertainties in μ lead to rates in the 2.5 - 3.8 EQ/100 yr^{-1} range and uncertainties in $\dot{s}_{f_{GEO}}$ lead to rates between 1.3 EQ/100 yr^{-1} and 5.0 EQ/100 yr^{-1}. The uncertainties in the coupled thickness $\langle cz \rangle$ in the GEO model have the most influence on the variability in earthquake rate, resulting in rates within the 2.0 - 5.5 EQ/100 yr^{-1} interval (Fig. 4).

6. Discussion

We used the SHIFT model (Bird and Liu, 2007) to determine the earthquake rates in the ED. SHIFT primarily relies on the assumption that the fundamental parameters for determining the earthquake rates of each fault or continuum element are comparable to those of the most similar plate boundary type (Bird and Kagan, 2004). This implies that the seismic characteristics of the most similar plate boundary type(s) (CCB and CTF for the ED) determined on a global scale (Bird and Kagan, 2004) are equivalent to those at the regional scale. This assumption is valid also for the faults not used in determining the average behaviour of the plate boundary type, such as the ED faults. As a consequence of the SHIFT assumptions, each individual fault can be considered to be a small plate boundary separating two infinitesimally small plates (the hanging wall and footwall blocks) and as such, its earthquake rate can be determined.

Due to a lack of available data, we cannot control the impact of regional parameters (e.g., the elastic shear modulus or the coupled thickness) on the earthquake rates in the ED with respect to the values obtained using the global parameters. We attempted to overcome these limitations by considering the effect of the parameter uncertainties determined by Bird and Kagan (2004). It should be noted that SHIFT predicts high corner magnitudes M^c_W and allows even short faults to host large earthquakes because it allows the ruptures to extend along the network of interconnected faults or to even form new fractures in the lithosphere (Bird and Liu,

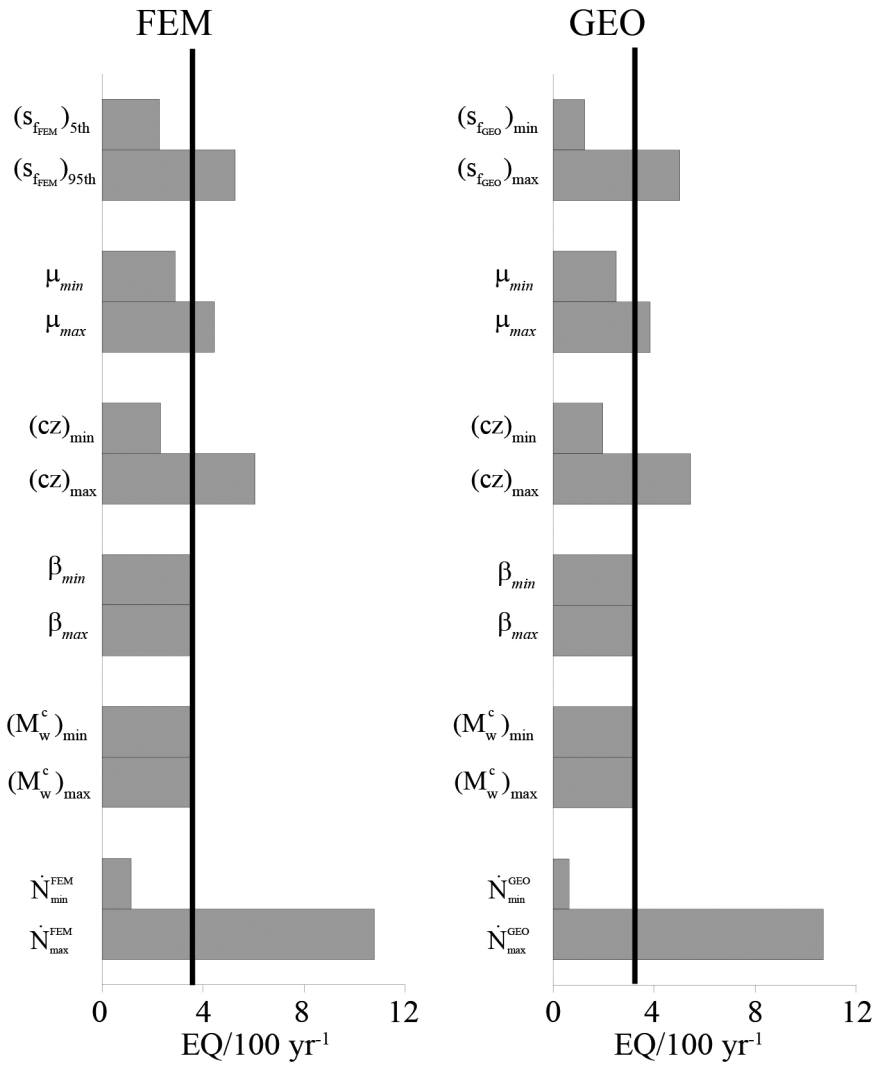

Fig. 4 - Earthquake rates sensitivity analyses respect to $\dot{s}_f$, μ, $\langle cz \rangle$, β and M_W^c uncertainties. The average earthquake rates for both models are presented as a thick black vertical line. The last two rows represent the absolute minimum ($\dot{N}_{FEM}^{min}$ and $\dot{N}_{GEO}^{min}$) and maximum earthquake rates ($\dot{N}_{FEM}^{max}$ and $\dot{N}_{GEO}^{max}$) obtained with the minimum and maximum value of each input parameter. Note that both FEM and GEO models result in comparable earthquake rates and that the most significant input parameters for earthquake rates variability are $\dot{s}_f$ and $\langle cz \rangle$, whereas β and M_W^c do not have a significant influence on the earthquake rates.

2007). This assumption represents a fundamental difference between the SHIFT hypothesis and a strictly "segmented-fault earthquake" type of model. In this work, we have shown that M_W^c and β do not play a significant role in earthquake rate variability in the ED. While the M_W^c and β uncertainties have a significant effect on the moment rate, they are largely self-cancelling when determining the number of M_W>5.66 earthquakes using a tapered Gutenberg-Richter distribution. Nonetheless, the earthquake rate variability in the FEM and GEO models is significant due to the ($\dot{s}_f$), μ and $\langle cz \rangle$ uncertainties. When these fundamental parameters become available on a regional scale (e.g., in the Mediterranean or peri-Adriatic region), it would be worthwhile to repeat all calculations presented in this work. Then it would be possible to

quantify the difference between the ED and the global characteristics of the CTF and CCB plate boundary types.

Our results can be compared with the earthquake rates determined by Bird *et al.* (2010) and Howe and Bird (2010). Howe and Bird (2010) developed a kinematic deformation model for the Mediterranean region and converted the long-term fault slip rates and distributed deformation rates into a set of long-term seismicity maps with threshold magnitudes M_W of 5.0, 6.0, 7.0 and 8.0. Bird *et al.* (2010) used the Global Strain Rate Map (Kreemer *et al.*, 2003) to forecast the long-term shallow seismicity of the Earth. In both studies, the total number of earthquakes is comparable and the distributions in Bird *et al.* (2010) and Howe and Bird (2010) have a more pronounced bulls-eye pattern than our results (Fig. 5). These differences may be due to the inclusion of GPS measurements in the studies of Bird *et al.* (2010) and Howe and Bird (2010). Bird *et al.* (2010) used the data from the Global Strain Rate Project as input and the role of GPS measurements is therefore straightforward. However, Howe and Bird (2010) relied on a kinematic ("inverse") model that simultaneously fits stress data, fault slip rates and GPS measurements. Kinematic models generally forecast seismicity better than dynamic models, such as the model of Kastelic and Carafa (2012), because they can usually fit several independent tectonic-related data sets reasonably well. This is not the case for permanent GPS data for the ED, as some of these data describe local non-tectonic phenomena unrelated to the long-term regional-scale velocity field (Kastelic and Carafa, 2012). The comparison of our results with those of Bird *et al.* (2010) and Howe and Bird (2010) suggests: 1) the importance of small-scale or regional dynamic modelling (FEM model) at this stage of data availability; and 2) the need to use available geological deformation indicators (GEO model). Future studies should rely on kinematic models that fit the different sets of independent data, but at this time, such

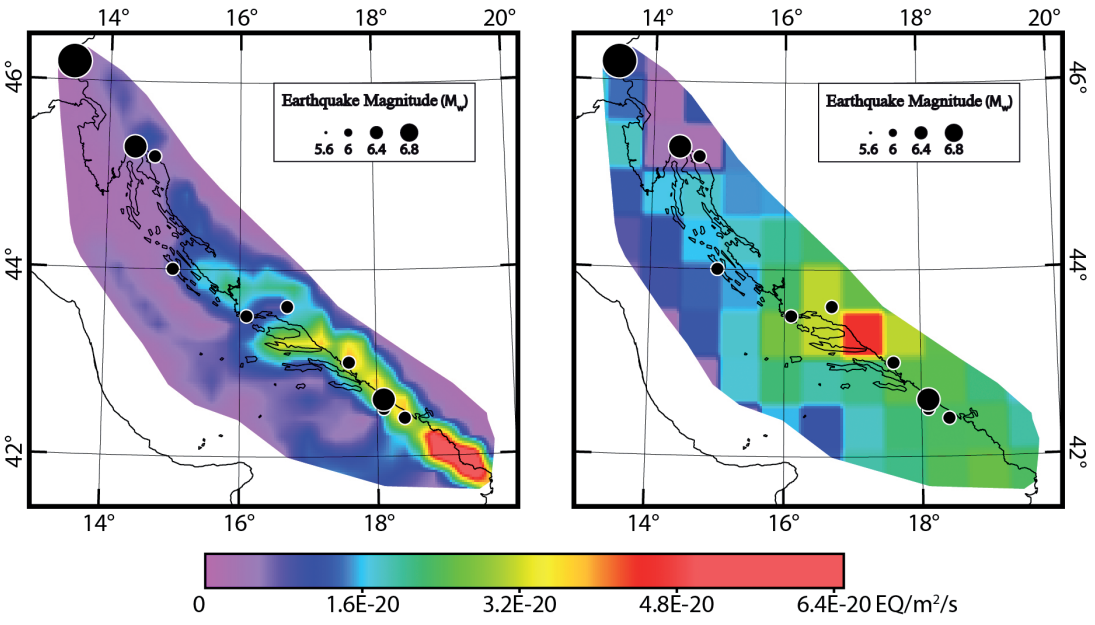

Fig. 5 - Comparison between: a) the FEM model presented in this study; and b) the kinematic model presented by Bird *et al.* (2010) for the ED for $M_W > 5.66$.

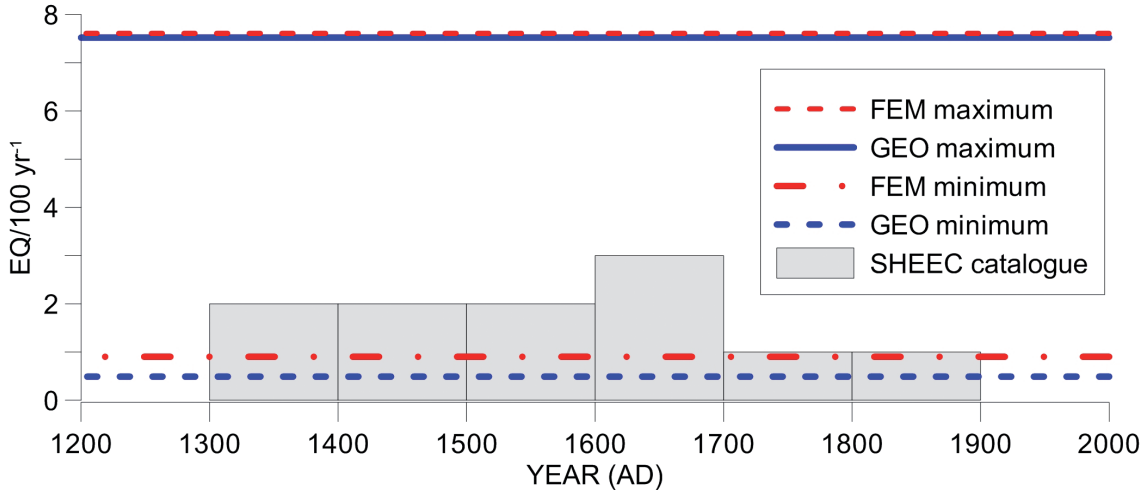

Fig. 6 - Comparison of earthquakes rates for M_W>5.8 from the FEM and GEO models and the SHEEC historic earthquake catalogue (Stucchi *et al.*, 2013).

models cannot satisfactorily reproduce the geodynamics and seismicity of the ED.

A retrospective comparison to establish the performance of our model can be carried out using historical and instrumental seismic catalogues (e.g., Karnik, 1971; Shebalin *et al.*, 1974; Herak *et al.*, 1996; Albini, 2004; Markušić, 2008; ANSS, 2012). These catalogues cover different time periods and were compiled using different criteria; simply merging them would be inappropriate. To overcome this drawback, we compared our earthquake rates to the SHEEC historical earthquake catalogue (Stucchi *et al.*, 2013) that homogenized various historical regional earthquake catalogues at the European scale for the AD 1000 - 1899 time interval. In this catalogue, special attention has been given to assessing the completeness of earthquake data in different areas. The ED lies mainly within the "J - Northern Italy" area, which has a magnitude of completeness of M_W 5.8 from year AD 1300. The SHEEC catalogue contains 11 $M_W > 5.8$ earthquakes for the ED for years AD 1300 - 1900 (see Fig. 5), corresponding to 1.8 earthquakes per century. To directly compare our results with the earthquakes reported in the SHEEC catalogue, we calculated the $M_W > 5.8$ earthquake rates and their related variability for both the FEM and GEO models. We obtained $\dot{N}^{\min}_{FEM}$ = 0.90 EQ/100 yr^{-1} and $\dot{N}^{\max}_{FEM}$ = 7.61 EQ/100 yr^{-1} for the FEM model and $\dot{N}^{\min}_{GEO}$ = 0.49 EQ/100 yr^{-1} and $\dot{N}^{\max}_{GEO}$ = 7.52 EQ/100 yr^{-1} for the GEO model (Fig. 6). The SHEEC catalogue earthquake rate for $M_W > 5.8$ in the ED falls within the uncertainty intervals of the GEO and FEM models. However we need to acknowledge that final FEM and GEO earthquake-rate uncertainties are wide as the input parameter uncertainties are significant.

We suppose that an earthquake catalogue-based, time-dependent model might outperform our earthquake rate estimates in a short-term test. However, our long-term earthquake rates are more valuable over longer periods, as aftershock swarms are included as a part of the background seismicity and the probability of earthquakes occurring in a geologically active, but historically silent faults increases. For the same time window used to check the consistency of the long-term average earthquake rates, new and more reliable data (slip rates, GPS velocities and SHmax orientations) should be available and the rates presented in this work should be updated

accordingly. The work presented in this study represents the first step in a lengthy process of better understanding the relationship between geodynamic models, data on geological active faults and earthquake rates.

Acknowledgements. This research was supported by the EU-EP7-funded project Seismic Hazard Harmonization in Europe SHARE (grant 226967) and by project MIUR-FIRB 'Abruzzo' (code: RBAP10ZC8K_003). We acknowledge the comments and remarks from the two anonymous referees that improved the quality and readability of the manuscript. A portion of the material presented in this paper was presented at the 30th Gruppo Nazionale di Geofisica della Terra Solida (GNGTS) meeting held in Trieste from November 14 to 17, 2011.

REFERENCES

Albini P.; 2004: *A survey of the past earthquakes in the eastern Adriatic (14th to early 19th century)*. Ann. Geophys., **47**, 675-703.

ANSS (Advanced National Seismic System); 2012: *Composite earthquake catalog*. Northern California Earthquake Data Center (NCEDC), Berkeley, CA, USA. <quake.geo.berkeley.edu/cnss/>, last accessed on May 10, 2012.

Basili R. and Kastelic V.; 2011: *D3.4 - Database of active faults and seismogenic sources*. Seismic Hazard Harmonization in Europe - SHARE project, Deliverable D3.4.

Basili R., Kastelic V., Demircioglu M.B., Garcia Moreno D., Nemser E.S., Petricca P., Sboras S.P., Besana-Ostman G.M., Cabral J., Camelbeeck T., Caputo R., Danciu L., Domac H., Fonseca J., García-Mayordomo J., Giardini D., Glavatovic B., Gulen L., Ince Y., Pavlides S., Sesetyan K., Tarabusi G., Tiberti M.M., Utkucu M., Valensise G., Vanneste K., Vilanova S. and Wössner J.; 2013: *The European Database of Seismogenic Faults (EDSF) compiled in the framework of the project SHARE*. doi:10.6092/INGV.IT-SHARE-EDSF. <diss.rm.ingv.it/share-edsf/>.

Bennett R.A., Hreinsdóttir S., Buble G., Bašić T., Bačić Ž., Marjanović M., Casale G., Gendaszek A. and Cowan D.; 2008: *Eocene to present sub-duction of southern Adria mantle lithosphere beneath the Dinarides*. Geol., **36**, 3-6, doi:10.1130/G24136A.1.

Bird P.; 2003: *An updated digital model of plate boundarie*. Geochem. Geophys. Geosyst., **4**, 1027, doi:10.1029/2001GC000252.

Bird P.; 2009: *Long-term fault slip rates, distributed deformation rates, and forecast of seismicity in the western United States from joint fitting of community geologic, geodetic, and stress direction data sets*. J. Geophys. Res., **114**, B11403, doi:10.1029/2009JB006317.

Bird P. and Kagan Y.Y.; 2004: *Plate-tectonic analysis of shallow seismicity: apparent boundary width, beta, corner magnitude, coupled lithosphere thickness, and coupling in seven tectonic settings*. Bull. Seismol. Soc. Am., **94**, 2380-2399.

Bird P. and Liu Z.; 2007: *Seismic hazard inferred from tectonics: California*. Seismol. Res. Lett., **78**, 37-48.

Bird P., Kagan Y.Y. and Jackson D.D.; 2002: *Plate tectonics and earthquake potential of spreading ridges and oceanic transform faults*. In: Stein S. and Freymueller J.T. (eds), Am. Geophys. Union, Washington, DC, USA, Plate Boundary Zones, Geodynamics Series, **30**, 203-218.

Bird P., Kagan Y.Y., Jackson D.D., Schoenberg F.P. and Werner M.J.; 2009: *Linear and nonlinear relations between relative plate velocity and seismicity*. Bull. Seismol. Soc. Am., **99**, 3097-3113, doi:10.1785/0120090082.

Bird P., Kreemer C. and Holt W.E.; 2010: *A long-term forecast of shallow seismicity based on the Global Strain Rate Map*. Seismol. Res. Lett., **81**, 184-194, doi:10.1785/gssrl.81.2.184.

Carafa M.M.C. and Barba S.; 2011: *Determining rheology from deformation data: the case of central Italy*. Tectonics, **30**, TC2003, doi:10.1029/2010TC002680.

Drobne K. and Pavlovec R.; 1991: *Paleocene and Eocene beds in Slovenia and Istria*. In: Drobne K. and Pavlovec R. (eds), Proc. Second meeting IGCP project 286, Introduction to the Paleogene of SW Slovenia and Istria Field Trip Guidebook, Postojna, Slovenia, pp. 7-17.

Ekström G. and Nettles M.; 1997: *Calibration of the HGLP seismograph network and centroid-moment tensor analysis of significant earthquakes of 1976*. Phys. Earth Planet. Inter., **101**, 221-246.

Ekström, G., M. Nettles, and A. M. Dziewonski; 2012: *The global CMT project 2004-2010: centroid-moment tensors for 13,017 earthquakes*. Phys. Earth Planet. Inter., **200-201**, 1-9, doi:10.1016/j.pepi.2012.04.002.

Grenerczy G., Sella G., Stein S. and Kenyeres A.; 2005: *Tectonic implications of the GPS velocity field in the northern Adriatic region*. Geophys. Res. Lett., **32**, L16311, doi:10.1029/2005GL022947.

Grünthal G. and Wahlström R.; 2012: *The European-Mediterranean Earthquake Catalogue (EMEC) for the last millennium*. J. Seismol., **16,** 535-570, doi:10.1007/s10950-0129302-y.

Herak M., Herak D. and Markušić S.; 1996: *Revision of the earthquake catalogue and seismicity of Croatia, 1908-1992*. Terra Nova, **8**, 86-94.

Howe T.C. and Bird P.; 2010: *Exploratory models of long-term crustal flow and resulting seismicity in the Alpine-Aegean orogen*. Tectonics, **29**, TC4023, doi:10.1029/2009TC002565.

Jackson D.D. and Kagan Y.Y.; 1999: *Testable earthquake forecasts for 1999*. Seism. Res. Lett., **70,** 393-403.

Kagan Y.Y. and Jackson D.D.; 2000: *Probabilistic forecasting of earthquakes*. Geophys. J. Int., **143**, 438-453**.**

Karnik V.; 1971: *Seismicity of the European area: Part I and Part II*. Reidel Publishing Company, Dordrecht, The Netherlands, 364 +218 pp.

Kastelic V. and Carafa M.M.C.; 2012: *Fault slip rates for the active External Dinarides thrust-and fold belt*. Tectonics, **31**, TC3019, doi:10.1029/2011TC003022.

Kastelic V., Vannoli P., Burrato P., Fracassi U., Tiberti M.M. and Valensise G.; 2013: *Seismogenic sources in the Adriatic domain*. Mar. Pet. Geol., **42**, 191-213, doi:10.1016/j.marpetgeo.2012.08.002.

Kreemer C., Holt W.E. and Haines A.J.; 2003: *An integrated global model of present-day plate motions and plate boundary deformation*. Geophys. J. Int., **154**, 8-34, doi:10.1046/j.1365-246X.2003.01917.x.

Markušić S.; 2008: *Seismicity of Croatia*. In: Husebye E.S. (ed), Earthquake monitoring and seismic hazard mitigation in Balkan countries, NATO Science Series, **81**, 81-98.

Pacheco J.F. and Sykes L.R.; 1992: *Seismic moment catalog of large, shallow earthquakes, 1900–1989,* Bull. Seism. Soc. Am. **82**, 1306-1349.

Rucker W.K.; 2009: *Neotectonic kinematic analysis of the Philippines orogen: regional strain-rates and a forecast of long-term seismicity*. M.S. thesis in Geology, University of California, Los Angeles, CA, USA, 56 pp.

Scrocca D.; 2006: *Thrust front segmentation induced by differential slab retreat in the Apennines (Italy)*. Terra Nova, **18**, 154-161, doi:10.1111/j.1365-3121.2006.00675.x.

Shebalin N.V., Karnik V. and Hadzievski D.; 1974: *Catalogue of earthquakes of the Balkan region*. In: Shebalin N.V., Karnik V. and Hadzievski D. (eds), UNDP-UNESCO, Survey of the seismicity of the Balkan region, Skopje, Macedonia, 600 pp.

Stucchi M., Rovida A., Gomez Capera A.A., Alexandre P., Camelbeeck T., Demircioglu M.B., Gasperini P., Kouskouna V., Musson R.M.W., Radulian M., Sesetyan K., Vilanova S., Baumont D., Bungum H., Fäh D., Lenhardt W., Makropoulos K., Martinez Solares J.M., Scotti O., Živčić M., Albini P., Batllo J., Papaioannou C., Tatevossian R., Locati M., Meletti C., Viganò D. and Giardini D.; 2013: *The SHARE European Earthquake Catalogue (SHEEC) 1000-1899*. Journal of Seismology, doi: 10.1007/s10950-012-9335-2.

Tari V.; 2002: *Evolution of the northern and western Dinarides: a tectonostratigraphic approach*. European Geosciences Union, Stephan Mueller Special Publication Series, **1** , 223-236.

Tari-Kovačić V.; 1998; *Geodynamics of the Middle Adriatic offshore area, Croatia, based on stratigraphic and seismic analysis of Paleogene beds*. Acta Geol. Hung., **41**, 313-326.

Tari-Kovačić V., Kalac K., Lučič D. and Benić J.; 1998: *Stratigraphic analysis of Paleogene beds in some off-shore wells (central Adriatic area, Croatia)*. In: Hottinger L. and Drobne K. (eds), Paleogene shallow benthos of the Tethys, 2, Dela-Opera SAZU 4, 32, pp. 203-242.

Corresponding author: Michele Carafa
Istituto Nazionale di Geofisica e Vulcanologia
Via Arcivescovado 8, 67100 L'Aquila, Italy
Phone: 0862709111 ; e-mail: michele.carafa@ingv.it